ADVANCES IN ATMOSPHERIC SCIENCES, VOL. 35, DECEMBER 2018, 1533–1546

• **Original Paper** •

The Spatial and Temporal Variability of Global Stratospheric Gravity Waves and Their Activity during Sudden Stratospheric Warming Revealed by COSMIC Measurements

Xiaohua XU[1,2], Daocheng YU[1], and Jia LUO*[1,3]

[1]*School of Geodesy and Geomatics, Wuhan University,* 129 *Luoyu Road, Wuhan* 430079*, China*

[2]*Collaborative Innovation Center for Geospatial Technology,* 129 *Luoyu Road, Wuhan* 430079*, China*

[3]*Key Laboratory of Geospace Environment and Geodesy, Ministry of Education,* 129 *Luoyu Road, Wuhan* 430079*, China*

(Received 7 March, 2018; revised 5 June 2018; accepted 11 June 2018)

ABSTRACT

This study investigates the spatial and temporal variability of global stratospheric gravity waves (GWs) and the characteristics of GW activity during sudden stratospheric warming (SSW) using the GPS radio occultation measurements from the COSMIC mission during September 2006 to May 2013. Corresponding to the COSMIC RO observational window and analysis method, GW potential energy (Ep) with vertical scales no shorter than ~2 km is resolved. It is found that the distributions of GW Ep over 20–30 km and 30–38 km show similar spatial and seasonal variations. The variations of GW Ep with altitude and latitude along the westerly wind are identified in different seasons over 60°–80°W. In the middle and high latitudes, seasonal cycles are distinct in the time–latitude and time–altitude distributions of GW activities, which show larger Ep in winters when westerly wind dominates and smaller Ep in summers when easterly wind dominates. The influence of quasi-biennial oscillation on GW activity is recognized in the tropics. GW Ep enhances closely following the occurrence of minor SSW events; while during major events, GW Ep may not enhance, and sometimes may even weaken, in the regions where reversals of zonal wind occur, probably caused by the filtering impact of the 0 m s^{-1} wind level on the GWs.

Key words: stratospheric gravity waves, GPS radio occultation, COSMIC, potential energy, sudden stratospheric warming

Citation: Xu, X. H., D. H. Yu, and J. Luo, 2018: The spatial and temporal variability of global stratospheric gravity waves and their activity during sudden stratospheric warming revealed by COSMIC measurements. *Adv. Atmos. Sci.*, **35**(12), 1533–1546, https://doi.org/10.1007/s00376-018-5053-1.

1. Introduction

It is well known that gravity waves (GWs) transport energy, momentum, and chemical and atmospheric constituents horizontally and vertically, and play a major role in atmospheric dynamics and global atmospheric circulation (Holton, 1983; Nappo, 2002; Fritts and Alexander, 2003; John and Kumar, 2012; Sato et al., 2012). GWs can be generated by various sources, such as orography, wind shear, atmospheric convection, spontaneous emissions of GWs from imbalanced flows in the lower atmosphere, and propagate to the middle and upper atmosphere under the effect of background wind (Uccellini and Koch, 1987; Ern et al., 2013). As altitude increases, the density of the atmosphere decreases and the amplitude of GWs increases gradually. In unstable processes, GWs break and dissipate, and deposit energy and momentum into the background flow, which influences the atmospheric circulation.

Sudden stratospheric warming (SSW) is an intense transient phenomenon in the stratosphere over the winter pole. During an SSW event, the polar vortex of westerly wind in the winter hemisphere slows down or even reverses direction in a few days, accompanied by a rise in stratospheric temperature by several tens of K. SSW events can be classified into major and minor cases according to whether they are accompanied by a reversal of zonal wind. During a minor event, the temperature gradient in the stratosphere between 60° latitude and the pole, on zonal average, becomes positive over a certain altitudinal range at or below the 10 hPa level (Ern et al., 2016). During a major event, additionally, the stratospheric zonal wind at 60° latitude reverses from eastward to westward at or below the 10 hPa level (Chandran et al., 2014). A major SSW is a strong warming characterized by a reversal of the zonal wind into easterly wind, and is typically observed in the Northern Hemisphere (NH) (McHall, 1992). A

* Corresponding author: Jia LUO
Email: jialuo@whu.edu.cn

minor SSW, meanwhile, does not lead to a reversal of the zonal wind. The background structure of the atmosphere and general circulation change dramatically within a short period of time during SSW events, thus affecting GW propagation and transmission in the middle atmosphere profoundly (Wang and Alexander, 2009).

In recent decades, many scholars have studied GWs using measurements from different observation systems, such as radiosonde (Wang and Geller, 2003; Zhang et al., 2010, 2013), radar (Tsuda et al., 1989), rocket soundings (Eckermann et al., 1995), lidar (Duck et al., 1998; Li et al., 2010) and limb- and nadir-scanning satellites (Fetzer and Gille, 1994; Wu and Waters, 1996, 1997; Alexander et al., 2008; Gong et al., 2012; John and Kumar, 2012; Hoffmann et al., 2013). The global positioning system (GPS) radio occultation (RO) technique can provide large amounts of atmospheric parameter profiles with global coverage, high vertical resolution and long-term stability (Kursinski et al., 1997; Anthes et al., 2008; Zhang et al., 2011; Xu et al., 2009, 2014), which are applicable in the study of GW activities (Wu and Waters, 1996, 1997; Nastrom et al., 2000; Tsuda et al., 2000, 2011; Ratnam et al., 2004a,b; de la Torre et al., 2006; Alexander et al., 2008a; Faber et al., 2013; Jia et al., 2015; Xu et al., 2016).

Tsuda et al. (2000) studied the global distribution of GW potential energy (Ep) using the GPS RO data from the GPS/Meteorology (GPS/MET) mission. They found that Ep was larger in the tropics and winter hemisphere, while it decreased at 25–30 km and increased monotonically above 30 km. Using Challenging Minisatellite Payload (CHAMP) data, Ratnam et al. (2004a, 2004b) studied the global GW activity in the stratosphere and during SSW events occurring in the Southern Hemisphere (SH). They found that Ep was high at tropical latitudes and midlatitudes during winter and, during SSW, it became three times higher than usual. The GPS/MET mission provided about 150 occultations per day under optimum conditions (Rocken et al., 1997), and the CHAMP mission provided approximately 100 occultations per day (Wang and Alexander, 2009). Both missions, however, had lower spatial resolution compared with the Constellation Observing System for Meteorology, Ionosphere and Climate (COSMIC) mission, which can provide 1000–2000 RO events every day (Teng et al., 2013). COSMIC RO data have been widely used to investigate GW activities since the mission was launched in 2006. Alexander et al. (2008a, 2008b) investigated the stratospheric GW activity in the NH winter and studied the equatorial GWs based on COSMIC RO data. Their results show evidence of interaction between vertically propagating, convectively generated GWs and the background mean flow. GW parameters other than Ep can be derived from GPS RO data too. Based on COSMIC RO data, Wang and Alexander (2010) estimated temperature amplitudes, wavelengths, intrinsic frequency and momentum flux, while Faber et al. (2013) obtained global distributions of horizontal GW wavelengths. Using observations from multi-satellite missions including COSMIC, CHAMP, High Resolution Dynamics Limb Sounder (HIRDLS) and Thermosphere–Ionosphere–Mesosphere Energetics and Dynamics (TIMED)/Sounding of the Atmosphere using Broadband Emission Radiometry (SABER), the GW activity during SSW in the NH winter was studied by Wang and Alexander (2009), revealing that GW amplitudes enhance in the stratosphere and weaken in the lower mesosphere during SSW events. Jia et al. (2015) studied the GW activity during SSW in the 2008 and 2009 NH winter with COSMIC observations. They found that enhancements of GW amplitudes occurred during the SSW events and propagated downward from higher altitudes during major events. Khan and Jin (2016) investigated the influence of GWs on the tropopause temperature, height and water vapor over the Tibetan Plateau based on COSMIC RO data, and found that GWs have impacts on the cold-point tropopause temperature and water vapor concentration in the stratosphere.

In the above studies, global GW activities for certain time periods and height intervals were investigated using GPS RO data. Although research on GW activities during SSW has been carried out based on RO data, the time periods concerned only include the NH winters of 2008 and 2009. In this work, using COSMIC RO data from the period of September 2006 to May 2013, the spatial and temporal variability of GWs globally between the tropopause and 38 km is studied. To understand the activities of GWs during SSW more thoroughly, the features of GWs during six major and six minor SSW events in the NH winters for all seven years are investigated.

The GW Ep is obtained from COSMIC RO dry temperature profiles in this paper, based on which the spatial and temporal structures of Ep over the globe are studied and the variabilities of Ep during SSW events are analyzed. The data and methods employed are introduced in section 2. In section 3, the results and discussion are presented, with conclusions drawn in section 4.

2. Data and methods

This paper uses COSMIC level 2 (v2010.2640) dry temperature profiles from September 2006 to May 2013 produced by the COSMIC Data Analysis and Archive Center (CDAAC) of the University Corporation for Atmospheric Research (UCAR) to investigate the seasonal and interannual variability of stratospheric GWs (http://cdaac-www.cosmic.ucar.edu). The vertical resolution of the COSMIC RO temperature profile is ~1 km and the accuracy of the temperature is sub-Kelvin (Wang and Alexander, 2010). The height range of the dry temperature profile is from near the ground up to 60 km, but the temperature typically exhibits increased noise at upper levels due to the a priori information used in the inversion process and the residual ionospheric effects (Wang and Alexander, 2009; Hindley et al., 2015). Although GW activity up to 50 km is analyzed using COSMIC RO dry temperature data, it has been indicated that the upper height level of the COSMIC temperature profiles most appropriate for GW study is below 40 km (Hindley et al., 2015). The GW Ep over the height interval 8–38 km is retrieved using COSMIC RO

dry temperature profiles in this study, and the Ep is given by:

$$\mathrm{Ep} = \frac{1}{2}\left(\frac{g}{N}\right)^2\left(\frac{T'}{\overline{T}}\right)^2 , \quad (1)$$

$$N^2 = \frac{g}{\overline{T}}\left(\frac{\partial \overline{T}}{\partial z} + \frac{g}{c_p}\right) . \quad (2)$$

where g is the gravitational acceleration, N is the Brunt–Väisälä frequency, c_p is the isobaric heating capacity, z is the height, and $\overline{T}$ and T' are the background temperature and temperature perturbations caused by GWs, respectively. The calculation of Ep is focused on obtaining T'. Each COSMIC temperature profile is composed of the background temperature ($\overline{T}$) and the temperature perturbations caused by GWs (T'). To get reliable estimates of temperature perturbations, the background temperature should firstly be removed, so T' can be calculated by

$$T' = T - \overline{T} , \quad (3)$$

where T is the raw COSMIC temperature. In order to obtain the temperature perturbations caused only by GWs, the background temperature should contain waves with longer wavelength such as Kelvin waves and planetary waves.

Following closely Wang and Alexander (2009, 2010), the daily COSMIC temperature profiles are divided into 10° × 15° latitude–longitude boxes between 8 and 38 km, with a vertical resolution of 0.2 km, and the mean temperature of each grid is calculated. The S-transform is used for the zonal mean temperature at each latitude and altitude, and the zonal wavenumbers 0–6 are obtained to represent the background temperature. This background temperature is interpolated back to the positions of raw COSMIC profiles and subtracted from T using Eq. (3) to obtain the temperature perturbations. Then GW Ep is calculated by Eqs. (1) and (2). The flow chart for calculating the GW Ep is shown in Fig. 1. The analysis can resolve GWs with vertical scales no shorter than ~2 km, which is twice the vertical resolution of the GPS RO data (Wang and Alexander, 2009).

To further analyze the temporal and spatial variations of the GW activities, daily Ep values are binned and averaged in 5° × 5° longitude–latitude grid cells, with a vertical resolution of 0.2 km. The global distribution of seasonal means of GW Ep for a certain height interval is obtained through averaging the gridded seasonal means of Ep values vertically. The zonally averaged monthly or seasonal Ep values at a certain latitude are obtained at each height level, and the vertical variation in Ep over that latitude can be revealed accordingly.

3. Results and analyses

3.1. *Longitude–latitude distribution of seasonal-mean GW Ep*

It is well known that orography, strong convection in the tropics, tropospheric jets in the midlatitudes and polar night jets in the polar regions play important roles in the excitation of GWs, and the troposphere is the main GW source region. Zhang et al. (2010, 2013) also indicated that, between 0° and 35°N, there are intensive GW sources lying in the intermediate region between the tropospheric and lower stratospheric segments—typically, in the height range of 10–18 km. Here, two height layers above the troposphere (20–30 km and 30–38 km) are selected to study the spatial and temporal variations of GWs in different altitudinal regions. The global distributions of the seasonal means of GW Ep for these two altitude ranges during the period 2006–13 are presented in Figs. 2 and 3, respectively. The seasons are categorized here as March–April–May (MAM), June–July–August (JJA), September–October–November (SON) and December–January–February (DJF).

Figure 2 suggests that, in the altitudinal range of 20–30 km, and for all four seasons, GW Ep is generally higher over tropical latitudes than over other regions. In the tropics, Ep is

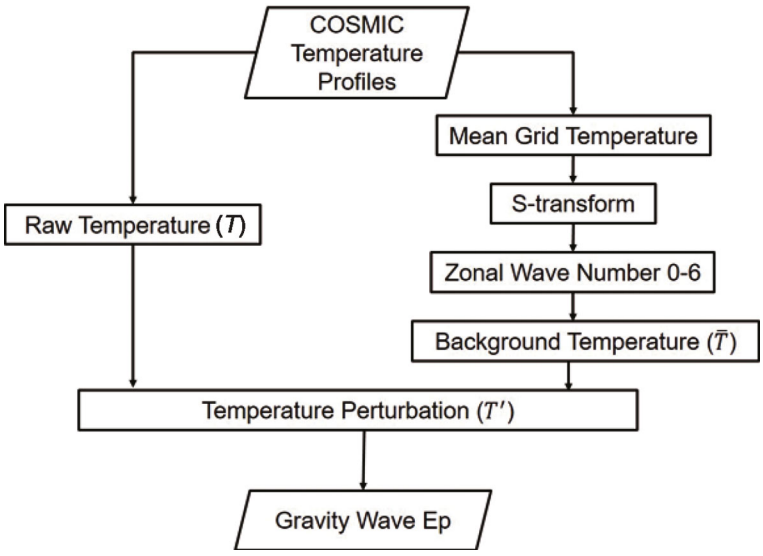

Fig. 1. Flow chart for calculating GW Ep.

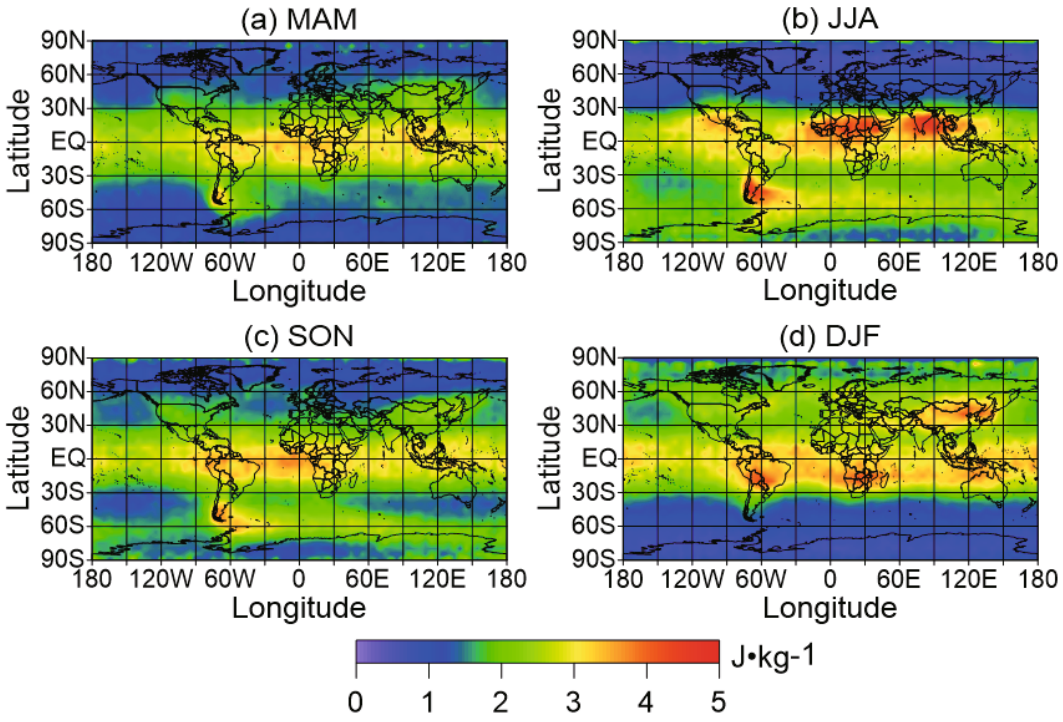

Fig. 2. Global distribution of 2006–13 averaged seasonal means [(a) MAM, (b) JJA, (c) SON, and (d) DJF] of GW Ep over 20–30 km.

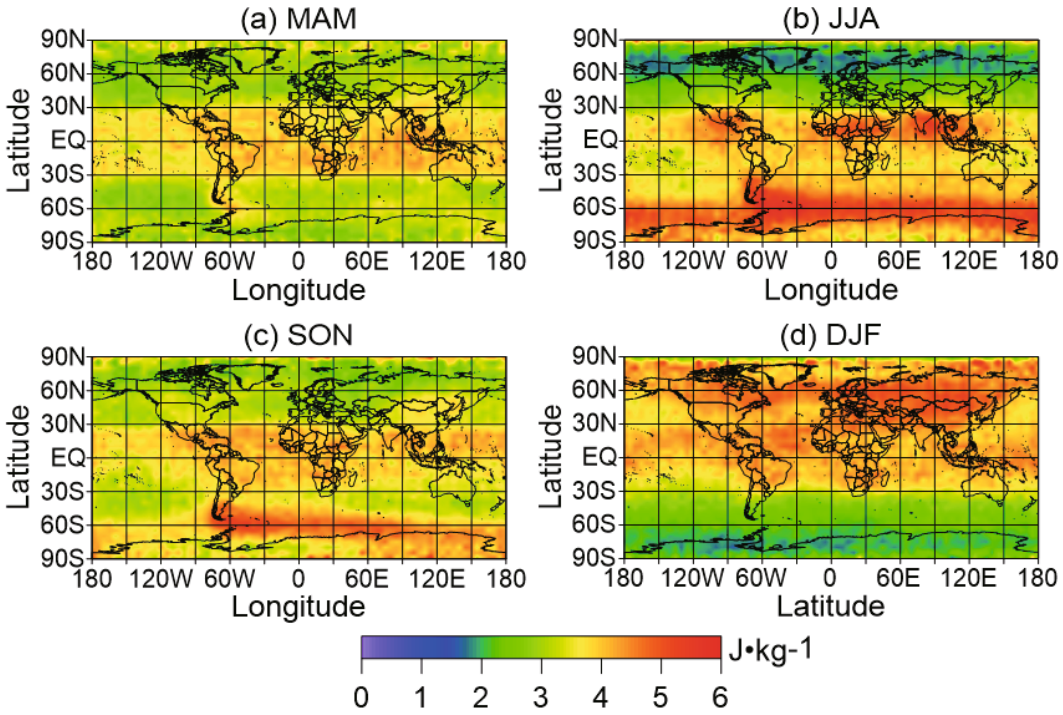

Fig. 3. Global distribution of 2006–13 averaged seasonal means [(a) MAM, (b) JJA, (c) SON, and (d) DJF] of GW Ep over 30–38 km.

symmetrical about the equator in MAM and SON, while it is larger/smaller north of the equator than south of the equator in JJA/DJF. The distribution of GW Ep over tropical latitudes is consistent with that of deep convection, which is the main source of GWs over the tropics (Ratnam et al., 2004a). The spatial distributions of the seasonal means of GW Ep in JJA and DJF in the seven years, as shown in Figs. 2b and d, are very similar to those in JJA and DJF of 2006, which are pre-

sented in Figs. 8c and d of Faber et al. (2013, p. 3177).

Comparison between Figs. 2b and d shows that, in JJA and DJF, higher values of GW Ep are obtained in the winter hemisphere than in the summer hemisphere in extratropical regions, which might be attributable to the influences of orography and zonal wind. The same seasonal cycle of GW activity and the attribution to different sources has also been found in other global satellite climatologies, e.g., AIRS/Aqua (Gong et al., 2012; Hoffmann et al., 2013).

Figures 2b and c show that, as detected in previous studies (Yan et al., 2010; Faber et al., 2013), in JJA and SON, the GW Ep is large over the southern Andes and decreases eastward. This might be because of the eastward propagation of the orographic mountain waves generated by the north–south distribution of the Andes (Alexander and de la Torre, 2010). Figure 2d shows that, in the NH winter, the Ep is large over the east of northern America (Faber et al., 2013), the Himalaya and other East Asian mountains, e.g. the Yablonoi Mountains, the Greater Khingan Mountains and the Sikhote-Alin.

Figure 3 shows that, at 30–38 km, there are large GW Ep values between 30°S and 30°N in all four seasons. Comparison between Figs. 2 and 3 indicates that the longitude–latitude distributional pattern of the seasonal-mean GW Ep at 30–38 km is similar to that at 20–30 km, while the magnitudes of Ep in these two altitudinal ranges differ. The Ep is generally larger at 30–38 km than at 20–30 km for each season, and the maximum Ep in the higher and lower altitudinal range is 6 J kg^{-1} and 5 J kg^{-1}, respectively. This agrees with Tsuda et al. (2000), who suggested that the Ep tends to become larger at midlatitudes within 30–40 km and shows a monotonic increase above 30 km.

3.2. *Latitude–altitude distribution of Ep in different seasons over 60°–80° W*

To investigate the vertical distribution of GWs in different seasons in detail, we take the longitudinal range of 60°–80°W , where the Andes are mainly located, as the study area in this part. In this longitudinal zone, seasonally averaged Ep values are obtained over each latitude at all the altitudinal levels between 8 km and 38 km, with an altitude grid of 0.2 km, based on which the zonal latitude–altitude variations of Ep values in different seasons are revealed accordingly. The latitude–altitude cross sections of 2006–2013 averaged seasonal means of GW Ep at 60°–80°W, together with the zonal wind distribution, are presented in Fig. 4.

Because GW Ep usually enhances in the tropopause region owing to the limitations of GW Ep calculation methods (Schmidt et al., 2008), studies about GW activities using GPS RO data are mainly concentrated within an altitudinal range from 1–2 km above the tropopause. Here, we focus on the GW activity above the tropopause height, which is about 17 km over the equator and decreases toward the polar regions, as shown in each subfigure of Fig. 4.

Figures 4a–d show that at 60°–80°W, in three of the four seasons, as the altitude increases from the tropopause, GW Ep generally decreases at first and reaches a minimum at around 20–30 km before then increasing. Figures 4b and d show that, in JJA and DJF, GW activity in this longitudinal region shows strong seasonal variation in the mid and high latitudes, with larger Ep in the winter hemisphere and smaller Ep in the summer hemisphere. Figure 4c shows that, in SON, GW Ep above the tropopause is larger in the SH than that in the NH for the longitudinal region of 60°–80°W.

Miyahara et al. (1986) reported that a strong background wind contributes to the upward propagation of GWs, and GW energy propagates not only upward but also poleward from the equatorial troposphere. Figures 4b–d show that the variations of GW Ep with altitude and latitude along the westerly wind are distinct in the SH during JJA and SON, and in the NH during DJF, which agrees with the findings of Alexander et al. (2008a) and Tsuda et al. (2000). As shown in Figs. 4b and c, GW Ep is generally large throughout the entire height range from the tropopause to 38 km between 60°S and 30°S, where the eastward wind is strong. From Figs. 4b and d, the Ep at 35–38 km even enhances over 60°–30°S and 60°–30°N, respectively, which might be attributable to the fact that the eastward wind at this height is strong enough to refract the GWs to longer vertical wavelengths so that they become visible to COSMIC (Hindley et al., 2015).

Figure 4b shows that, in JJA, westward wind dominates between 30°N and 90°N above an altitude of around 20 km. At this height, GW Ep is small too, which to some extent indicates the reason why the Ep in JJA shown in Figs. 2b and 3b is small in the mid and high latitudes of the NH. Figure 4d shows that, in DJF, the GW Ep at altitudes above the tropopause to the south of 30°S is generally smaller than that to the north of 30°N, which is consistent with Figs. 2d and 3d.

3.3. *Time–latitude distribution of Ep in different altitudinal regions*

To further study the interannual variation of GW activity over different latitudes and to understand the relationship between GW activity and zonal wind more deeply, the GW Ep and wind fields during September 2006 to May 2013 are averaged over longitudes for the two altitude ranges, 20–30 km and 30–38 km, and the results are shown in Figs. 5a and b.

Figure 5a shows that the GW Ep and zonal wind both show a clear seasonal cycle. At mid and high latitudes in the NH, the Ep over 20–30 km tends to be large during November–March, when the background wind is eastward, and small during May–September, when the background wind is westward. In comparison, at mid and high latitudes in the SH, the peak and minimum values of Ep over 20–30 km are observed during May–September and December–February, respectively. These results are consistent with previous works (Ratnam et al., 2004a; de la Torre et al., 2006). Moreover, the eastward wind is stronger and lasts longer in the winter seasons of the SH than in the winter seasons of the NH, which might be the reason why stronger GW activity exists in the winter seasons of the SH—a suggestion that is consistent with the findings of de la Torre et al. (2006).

It can be seen from Fig. 5a that westward wind is domi-

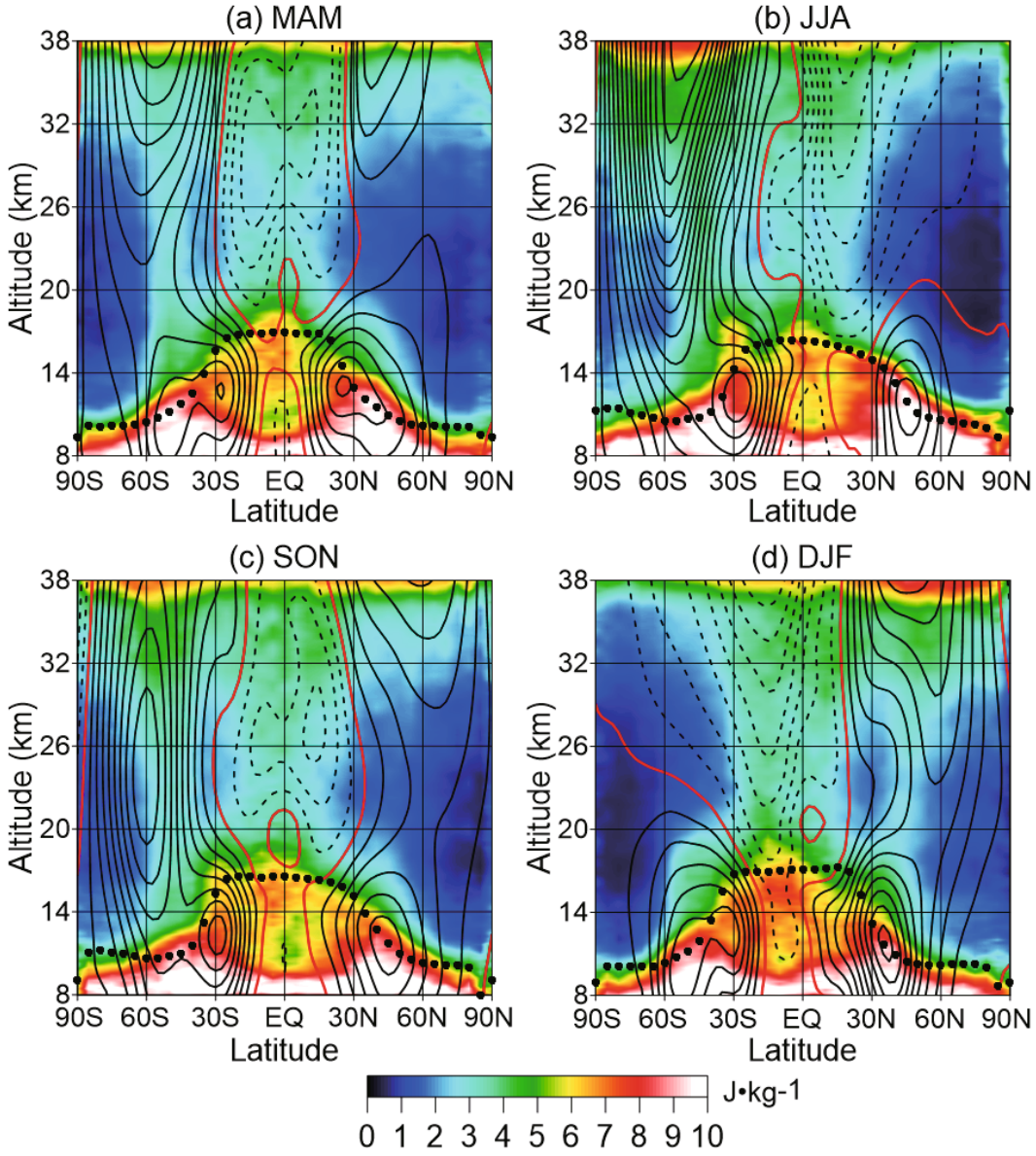

Fig. 4. Latitude–altitude cross sections of 2006–13 averaged seasonal means [(a) MAM, (b) JJA, (c) SON, and (d) DJF] of Ep and zonal wind at 60°–80°W. The eastward wind is represented by black solid lines, the westward wind is represented by black dashed lines, and the 0 m s^{-1} wind level is represented by red solid lines. The lapse rate tropopause height is represented by black dotted lines. Zonal wind data from ERA-Interim are used.

nant between 30°S and 30°N, and the effect of quasi-biennial oscillation (QBO) can be clearly detected in the temporal variation of both GW activity and zonal wind, which again is consistent with de la Torre et al. (2006). GW Ep enhances distinctly over the tropics in January 2008, July 2010 and January 2013, and the zonal wind direction changes from westward to eastward after each of these GW Ep enhancements.

The interannual variation of GW activity at 30–38 km shown in Fig. 5b is similar to that at 20–30 km shown in Fig. 5a, while the GW Ep is larger at 30–38 km than at 20–30 km in general. In each hemisphere, the seasonal cycle of the GW activity at 30–38 km is distinct over mid and high latitudes, with the peaks of Ep values observed in the winter seasons and the minima in the summer seasons. The influence of QBO can also be recognized in the interannual variations of GW activity and zonal wind at 30–38 km over tropical and subtropical latitudes (30°S–30°N) in Fig. 5b.

Normally, eastward wind is dominant in the winter hemisphere, but both Fig. 5a and b show that, during winters in regions north of 60°N, westward wind, which has distinct impacts on the variation of GW Ep, exists in January 2009, January 2010 and January 2013, and this might be the result of SSW. Major SSW events, which mainly occur in the NH (Labitzke and Naujokat, 2000), can lead to a reversal of the

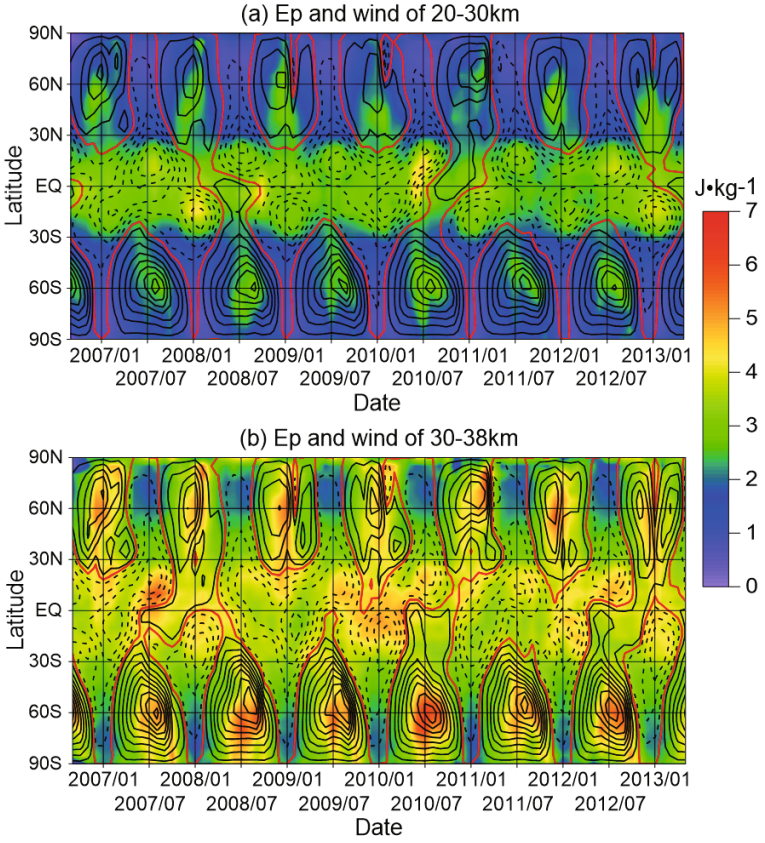

Fig. 5. Time–latitude plots of monthly means of Ep at (a) 20–30 km and (b) 30–38 km. The eastward wind is represented by black solid lines, the westward wind is represented by black dashed lines, and the 0 m s^{-1} wind level is represented by red solid lines. Zonal wind data from ERA-Interim are used.

zonal mean circulation (Ratnam et al., 2004b).

3.4. *Time–altitude distribution of Ep at typical latitudes*

To investigate the temporal variation in the vertical structure of GW Ep at typical latitudes more thoroughly, we present the time–altitude distribution of Ep at four latitudes (65°N, 0°, 50°S and 80°S) in Figs. 6a–d.

Figure 6a shows that GW activity in the altitude range from the tropopause to 38 km over 65°N presents a distinct seasonal cycle, with peaks observed in winter months when westerly wind is dominant, and minima observed in summer months when easterly wind is dominant. The maximum GW Ep is obtained at 35–38 km in the NH winter, and the minimum appears at 20–26 km in the NH summer. The 0 m s^{-1} wind level, which might result from SSW, is noticeable at around January 2009, January 2010 and January 2013.

The interannual variations of GW activity over 50°S and 80°S are shown in Figs. 6c and d. It can be seen that the seasonal cycle in the SH is as remarkable as that in the NH, while the peaks of Ep over 50°S and 80°S appear during JJA under the control of westerly wind. John and Kumar (2012) also detected this phenomenon using TIMED/SABER observations.

Sections 3.1–3.3 show that GW is less active in the summer hemisphere than in the winter hemisphere at mid and high latitudes. Figures 6a, c and d demonstrate clearly that the seasonal variations of Ep and zonal wind are consistent with each other, which shows that the change in the direction of zonal wind from eastward to westward and the accompanying filtering effects on GWs in summer seasons might be a possible mechanism underlying the GW seasonal variability at these latitudes.

Figure 6b shows that, over the equator, the GW Ep is generally low in regions where westward wind is dominant, and a QBO of Ep is observed between the tropopause height and 38 km. de la Torre et al. (2006) observed Ep QBO using CHAMP/GPS data. John and Kumar (2012) reported lower-stratospheric GW Ep QBO using TIMED/SABER observations. It is evident that, in the QBO region, the maximum values of Ep are observed where the wind direction changes from westward to eastward, which might be attributable to the fact that stratospheric wind systems selectively filter GWs having horizontal phase speeds that are the same as the background wind speeds (John and Kumar, 2012).

3.5. *Variability of Ep during SSW*

3.5.1. *Time–latitude variability of Ep during SSW*

As mentioned previously (section 3.3), during winters, westward wind can be found north of 60°N, which might be attributable to the impacts of SSW events. In this part, we in-

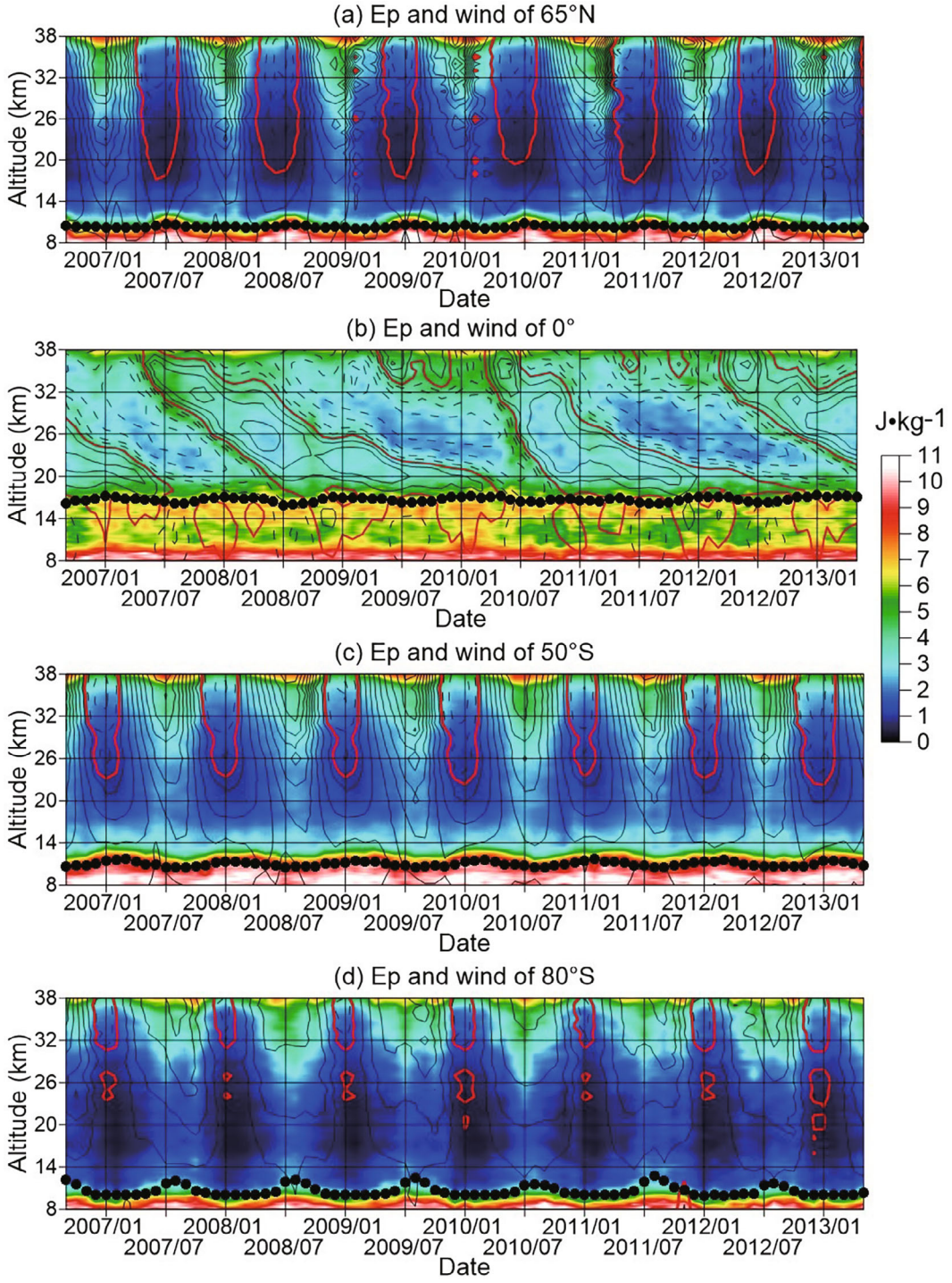

Fig. 6. Time–altitude plots of monthly means of Ep for (a) 65°N, (b) 0°, (c) 50°S, and (d) 80°S. The eastward wind is represented by black solid lines, the westward wind is represented by black dashed lines, and the 0 m s^{-1} wind level is represented by red solid lines. The lapse rate tropopause height is represented by black dotted lines. Zonal wind data from ERA-Interim are used.

vestigate the features of GW activity during the periods when the reversal of background wind occurs.

Figure 7 shows the time–latitude contours of composited daily mean temperature and composited daily mean Ep and zonal wind at 20–30 km during major and minor SSW events in 2007–13. Definition-wise, SSW events during which the zonal winds at 60° reverse from eastward to westward at the 10 hPa level (around 32 km) are classified as major events. For convenience of illustration, the time period for each event shown here is from several days before the onset of the event to several days after the end of the event. Note, however, the major SSW event that occurred in 2011 is an exception, for

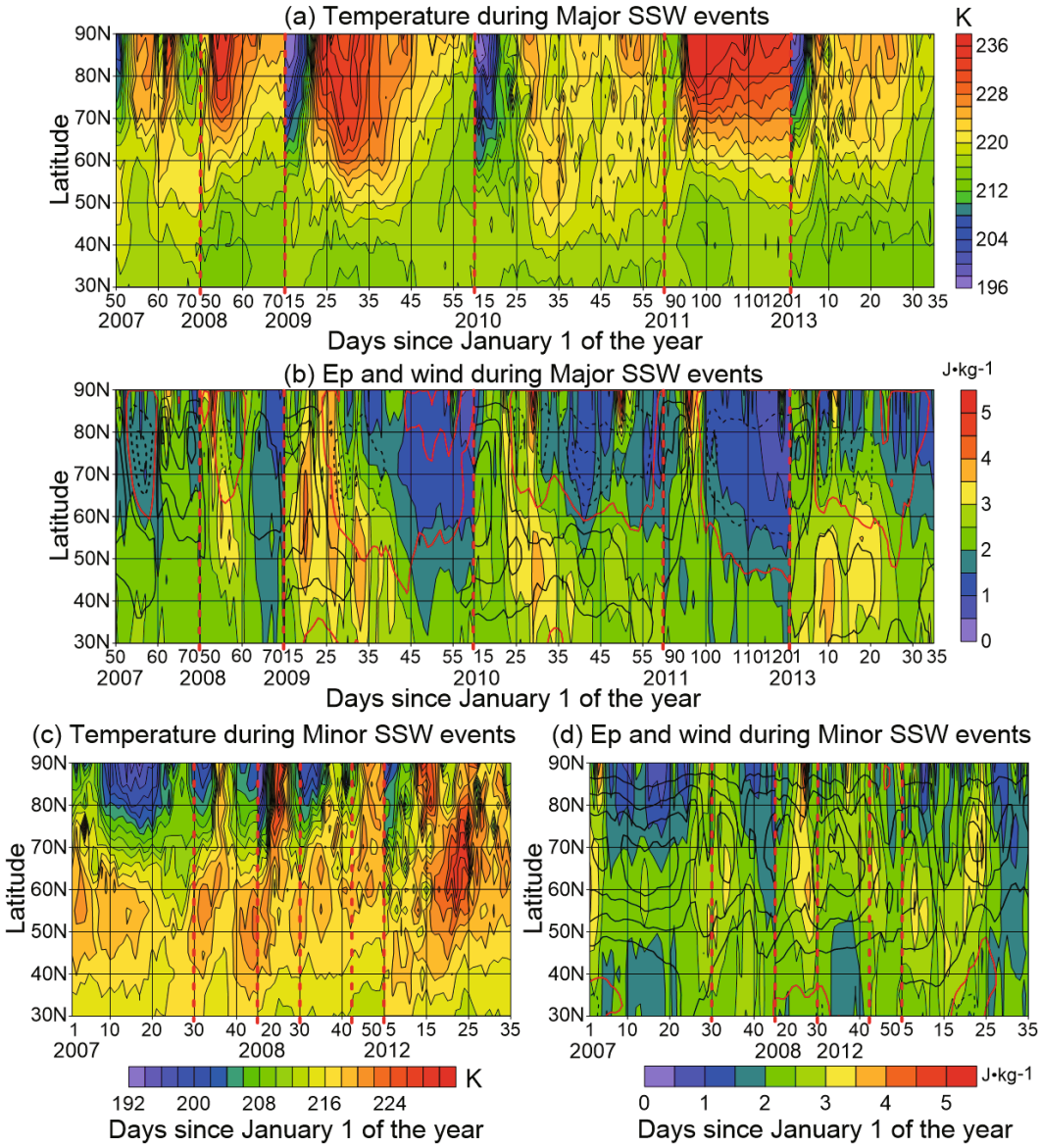

Fig. 7. Time–latitude contours of composited daily mean (a) temperature during major SSW events, (b) Ep and zonal wind during major SSW events, (c) temperature during minor SSW events, and (d) Ep and zonal wind during minor SSW events, at the altitudinal range of 20–30 km. Different events are separated by red dashed lines. The eastward wind is represented by black solid lines, the westward wind is represented by black dashed lines, and the 0 m s^{-1} wind level is represented by red solid lines. Zonal wind data from ERA-Interim are used.

which we just show part of the event's time span here. This is because that event lasted for more than two months, during which the variation in Ep and zonal wind was similar to the selected time span. Figures 7a and b show six major SSW events as having occurred during 2007 to 2013. All of these events are accompanied by the reversal of background wind.

Figure 7a shows that, during the period from 19 February to 11 March 2007, the Arctic stratospheric temperature increases intensely from 21 February to 6 March, which implies the occurrence of an SSW event. The warming propagates gradually from the Arctic region to the midlatitudes. Although there are precise definitions of major and minor SSW events, to define them in a simpler way is acceptable here because we are mainly studying the GW activities during SSW, rather than the event itself. So, this SSW event can be represented by the date of 4 March, and is identified as a major one because the background wind reverses, as shown in Fig. 7b. This figure also shows that the GW Ep decreases under the control of easterly wind in the 4 March major event, which might be attributable to the fact that the easterly wind caused by the major SSW event hinders the increase in Ep.

It can be seen from Fig. 7a that, during 19 February to 10 March 2008, the temperature over the Arctic region is low until late February, and then warms up, leading to a major SSW event on 24 February. Comparison between Fig. 7a and b shows that, during this major SSW event, the Ep enhances

just before the time when the 0 m s^{-1} wind level appears, and then propagates along it to midlatitudes. Within the 0 m s^{-1} wind level, where the zonal wind blows westward, the degree of Ep enhancement declines. The Ep becomes even smaller after the major event.

A pronounced major SSW event, which can be identified as the 23 January 2009 event, is significantly discernible in Fig. 7a. Figure 7b shows that, during this event, the 0 m s^{-1} wind level appears between 80°N and 90°N a little later than the onset time of the SSW event, and then propagates to midlatitudes. The accompanying enhancement of Ep over the Arctic region appears on 20 January, when the major event begins, and continues to 28 January. Then, the enhancement of Ep extends along the 0 m s^{-1} wind level to midlatitudes. Within the 0 m s^{-1} wind level, the direction of the zonal wind field changes to westward and the enhancement of Ep declines. Ep becomes even smaller as the major event ends.

Three other major SSW events can be identified from Figs. 7a and b, on 29 January 2010, 8 April 2011, and 8 January 2013, respectively. During all three events, the 0 m s^{-1} wind level appears almost at the same time as when the stratospheric temperature begins to increase suddenly, and the GW Ep generally decreases within the 0 m s^{-1} wind level, which is controlled by easterly wind. Figure 7b shows that, during the 29 January 2010 major event, the enhancement of Ep occurs along the 0 m s^{-1} wind level, and this enhancement extends to the midlatitudes. Over 60°–90°N, the GW Ep is distinctly large during 20–30 January; while over 30°–60°N, the significantly large values of Ep are obtained during 20 January to 9 February. GW Ep enhances in the Arctic regions around 19 February. During the 18 April 2011 major event, the enhancement of Ep occurs where the 0 m s^{-1} wind level appears, and Ep decreases in the easterly wind regime; while during the 8 January 2013 major event, significant enhancement of Ep only occurs to the south of the 0 m s^{-1} wind level.

Figures 7c and d show six minor SSW events as having occurred during 2007–13, i.e., without zonal wind reversal. Figure 7c shows that, during the two 2007 minor events, i.e., 2 January and 6 February, the Arctic stratospheric temperature increases intensely, which is accompanied by an enhancement of GW activity. The GW Ep enhancement extends to the midlatitudes, which can be seen from Fig. 7d. During the other four minor events, on 25 January, 5 February and 15 February 2008, and 23 January 2012, respectively, the warming is accompanied by Ep enhancement.

3.5.2. *Time–altitude variability of Ep during SSW*

Figure 8 shows the time–altitude contours of composited daily mean temperature and composited daily mean Ep and zonal wind over 60°N and 90°N during major and minor SSW events in 2007–13. The selected time spans for the SSW events are the same as those shown in Fig. 7.

Comparison between Fig. 8a and b indicates that the downward progressions of warming are distinct in the 4 March 2007 major event. During this event, GW Ep decreases in the 0 m s^{-1} wind level. One major SSW event, on 24 February 2008, can be identified in Fig. 8a, and is also revealed in Fig. 7a. Comparison between Fig. 8a and b shows that the enhancement of GW Ep is not distinct during this major event, which is accompanied by zonal wind reversal.

The major SSW event on 23 January 2009 revealed in Fig. 7a is also identifiable in Fig. 8a. Comparison between Fig. 8a and b shows that the zonal wind reversal occurs later than the onset time of this SSW event, and GW Ep enhances in accompaniment to the occurrence of this event. The enhancement of Ep extends along the 0 m s^{-1} wind level to lower altitudes.

As in Figs. 7a and b, Figs. 8a and b show that, during the two major SSW events of 29 January 2010 and 8 April 2011, respectively, strong zonal wind reversals accompany the occurrence of these two events, which extends to the altitude of 8 km. During both events, GW Ep enhances at the onset of the 0 m s^{-1} wind level. However, within the 0 m s^{-1} wind level, where easterly wind dominates, GW Ep shows no enhancement, as in 2010, or even subsides, as in 2011.

A reversal of zonal wind accompanies the occurrence of the 8 January 2013 major SSW event, which we have already identified in Figs. 7a and b. During the easterly wind regime, no clear Ep enhancement occurs. As the SSW event ends, the GW activity quietens.

From Figs. 8c and d, the downward progressions of warming are distinct in the two minor SSW events of 2 January and 6 February 2007. During these two events, the enhancement of Ep is distinct. Three minor events, on 25 January, 5 February and 15 February 2008, respectively, are presented in Fig. 7c, and are also shown in Fig. 8c. Two of them, however—the 5 and 15 February events—are not very obvious in Fig. 7c, which is because they mainly occur over 30 km. Figure 8d reveals that GW Ep enhances distinctly during these three events. The 23 January 2012 SSW event, which is identifiable in Figs. 7c and d, is also distinguishable in Figs. 8c and d. In this event, although easterly wind appears during 12–18 January, the reversal of zonal wind occurs earlier than the warming. The enhancement of Ep still occurs, during 20–25 January, and the enhancement extends to the height of 20 km.

4. Discussion

The above analyses of the features of GW activities during SSW events occurring in the seven years from 2007 to 2013 show that:

(1) The reversals of zonal winds during the winters in regions north of 60°N, which are shown in Figs. 5, 6a and 7a, might be caused by major SSW events.

(2) During minor SSW events, GW Ep enhances, and the enhancement extends to mid or lower altitudes; while during major events, Ep enhances before or around the 0 m s^{-1} wind level and the enhancement extends along it to midlatitudes or downward. In the regions where reversals of zonal wind occur and easterly wind dominates, there is no significant enhancement of Ep; in fact, a subsiding of Ep is even possible, which might be due to the filtering impact of the 0 m s^{-1} wind

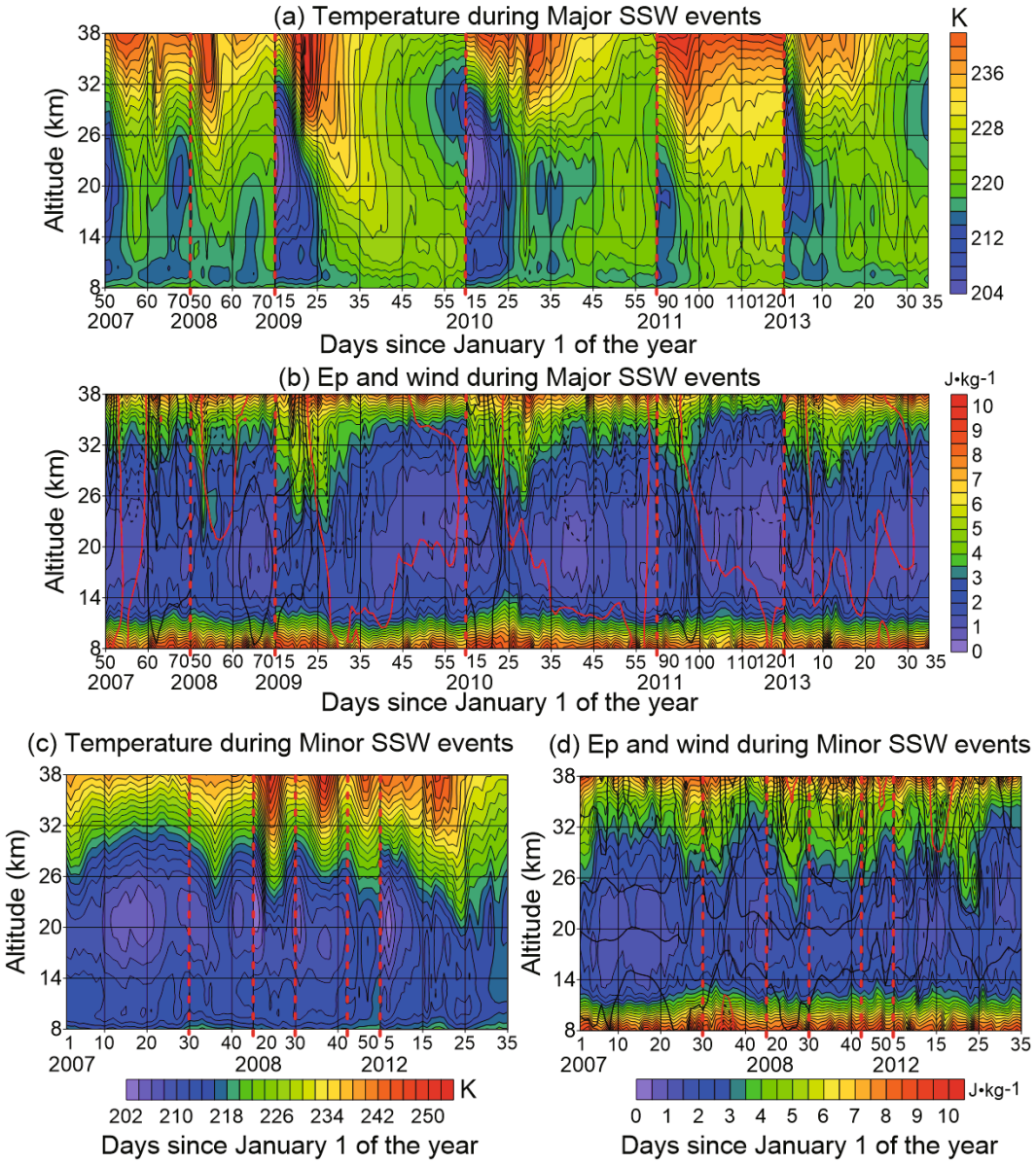

Fig. 8. Time–altitude contours of composited daily mean (a) temperature during major SSW events, (b) Ep and zonal wind during major SSW events, (c) temperature during minor SSW events, and (d) Ep and zonal wind during minor SSW events, over the latitudinal region of 60°–90°N. Different events are separated by red dashed lines. The eastward wind is represented by black solid lines, the westward wind is represented by black dashed lines, and the 0 m s^{-1} wind level is represented by red solid lines. Zonal wind data from ERA-Interim are used.

level on the GWs. Wang and Alexander (2009) also reported that orographically generated stationary GWs would be absorbed by the mean atmosphere as they approach the zero mean zonal wind level in the course of an SSW event.

(3) With the end of an SSW event, GW Ep decreases.

It has been noticed that GW activity usually enhances during SSW events (Ratnam et al., 2004b; Wang and Alexander, 2009; Jia et al., 2015; Ern et al., 2016). Ratnam et al. (2004b) used CHAMP/GPS data to analyze the GW activity during SSW in the SH and found that GW Ep is higher than normal during the warming. Using COSMIC, CHAMP, HIRDLS and TIMED/SABER observations, Wang and Alexander (2009) detected four SSW events in the 2007/08 NH winter, which is similar to our results here, and found that GW temperature amplitudes enhanced during the SSW events. Jia et al. (2015) studied the GW activity during SSW events in the 2008 and 2009 NH winter with COSMIC RO observations, and found that enhancements of GW amplitudes occurred during the events. They also found that, during major events, the enhancements of GW amplitudes extended downward from higher altitudes, which corresponded well with the vertical variations of the zonal wind reversals, and the enhancements seemed to occur at the same time as the wind reversal. Using HIRDLS and SABER satellite observations, Ern et al. (2016)

investigated the middle-atmosphere GW absolute momentum flux and its potential drag during SSW events of NH polar winters from 2001/02 to 2013/14. They found that sometimes GW activity is enhanced before or around the central date of major SSW events, and is strongly suppressed when the wind has reversed from eastward to westward. Our results are consistent with these studies.

5. Conclusions

In this study, GW Ep derived from COSMIC RO dry temperature profiles is used to study the spatial and temporal variability of stratospheric GWs over the globe during September 2006 to May 2013 and the features of GW activity during SSW events.

GW Ep is calculated following closely the methods of Wang and Alexander (2009, 2010), based on which the longitude–latitude distribution of the seasonal means of stratospheric GW Ep in two different altitudinal regions, the latitude–altitude distribution of Ep in different seasons over certain longitude regions, the time–latitude distribution of Ep in different altitudinal regions, the time–altitude distributions of Ep at typical latitudes, and the variability of GWs during SSW events mainly occurring in the NH winters of the seven years are investigated.

The global distributions of the stratospheric GW Ep over the two altitudinal regions (20–30 km and 30–38 km) show similar spatial and seasonal variations. Large Ep values exist over the tropical region, associated with deep convection, and the southern Andes and Antarctic peninsula, where orographic GWs occur. The GW activities are stronger in the winter hemisphere than in the summer hemisphere, and generally enhance in the higher altitudinal range.

From the latitude–altitude distributions of GW Ep in different seasons over 60°–80°W, the vertical distribution of GW can be clearly identified and the seasonal variation of GW can be understood. The variations of GW Ep with altitude and latitude along the westerly wind from the subtropical tropopause to the upper stratosphere can aid our understanding as to why the averaged means of Ep at 20–30 km are commonly smaller than those at 30–38 km. The time–latitude distributions of GW Ep at 20–30 km and 30–38 km both show distinct seasonal cycles over mid and high latitudes, which corresponds to the seasonality of zonal wind. In each hemisphere, the peaks of Ep values are observed in winter seasons, when eastward wind dominates, and the minima are in summer seasons, when westward wind dominates, which is consistent with previous works (Ratnam et al., 2004a; de la Torre et al., 2006). Moreover, the eastward wind is stronger and lasts longer in the winter seasons of the SH than in the winter seasons of the NH, which might be a factor leading to stronger GW activity in the winter seasons of the SH.

The time–altitude distributions of Ep at four typical latitudes (65°N, 0°, 50°S and 80°S) further reveal that the underlying mechanism responsible for the fact that GW is less active in the summer hemisphere than in the winter hemisphere at mid and high latitudes might be that the change in the direction of the zonal wind from eastward in the lower stratosphere to westward at higher altitude in the summer seasons filters out most of the orographic GWs at these latitudes; while at the equator, there is a distinct QBO in GW activity and the maximum Ep is obtained around the 0 m s^{-1} wind level (John and Kumar, 2012).

The analyses of GW activity in SSW events occurring mainly during NH winters show that, during all minor events, the enhancements of GW Ep are detected closely after the occurrence of the events; while during major events, GW Ep enhances before or around the 0 m s^{-1} wind level and the enhancement extends along this level to midlatitudes or to lower altitudes. GW Ep may not enhance, and sometimes may even weaken, in the regions where reversals of zonal wind occur and easterly wind dominates, which might be caused by the filtering impact of the 0 m s^{-1} wind level on the GWs (Ratnam et al., 2004b; Wang and Alexander, 2009; Jia et al., 2015; Ern et al., 2016).

Acknowledgements. This work was supported by the National Natural Science Foundation of China (Grant Nos. 41774033 and 41774032). The authors would like to thank UCAR for providing the COSMIC RO data via CDAAC, and the ECMWF for providing the zonal wind data.

REFERENCES

Alexander, M. J., and Coauthors, 2008: Global estimates of gravity wave momentum flux from High Resolution Dynamics Limb Sounder observations. *J. Geophys. Res*., **113**(D15), D15S18, https://doi.org/10.1029/2007JD008807.

Alexander, P., and A. de la Torre, 2010: A method to infer the three Cartesian wavelengths of a mountain wave from three soundings. *Journal of Applied Meteorology and Climatology*, **49**(9), 2069–2074, https://doi.org/10.1175/2010JAMC2348.1.

Alexander, S. P., T. Tsuda, and Y. Kawatani, 2008a: COSMIC GPS observations of Northern Hemisphere winter stratospheric gravity waves and comparisons with an atmospheric general circulation model. *Geophys. Res. Lett*., **35**(10), L10808, https://doi.org/10.1029/2008GL033174.

Alexander, S. P., T. Tsuda, Y. Kawatani, and M. Takahashi, 2008b: Global distribution of atmospheric waves in the equatorial upper troposphere and lower stratosphere: COSMIC observations of wave mean flow interactions. *J. Geophys. Res*., **113**(D24), D24115, https://doi.org/10.1029/2008JD010039.

Anthes, R. A., and Coauthors, 2008: The COSMIC/FORMOSAT-3 mission: Early results. *Bull. Amer. Meteor. Soc*., **89**(3), 313–334, https://doi.org/10.1175/BAMS-89-3-313.

Chandran, A., R. L. Collins, and V. L. Harvey, 2014: Stratosphere-mesosphere coupling during stratospheric sudden warming events. *Advances in Space Research*, **53**(9), 1265–1289.

de la Torre, A., T. Schmidt, and J. Wickert, 2006: A global analysis of wave potential energy in the lower stratosphere derived from 5 years of GPS radio occultation data with CHAMP. *Geophys. Res. Lett*., **33**(24), L24809, https://doi.org/10.1029/2006GL027696.

Duck, T. J., J. A. Whiteway, and A. I. Carswell, 1998: Lidar observations of gravity wave activity and Arctic stratospheric vor-

tex core warming. *Geophys. Res. Lett*., **25**(15), 2813–2816, https://doi.org/10.1029/98GL02113.

Eckermann, S. D., I. Hirota, and W. K. Hocking, 1995: Gravity wave and equatorial wave morphology of the stratosphere derived from long-term rocket soundings. *Quart. J. Roy. Meteor. Soc*., **121**(521), 149–186, https://doi.org/10.1002/qj.49712152108.

Ern, M., and Coauthors, 2013: Observations and ray tracing of gravity waves: Implications for global modeling. *Climate and Weather of the Sun-Earth System* (*CAWSES*), F. J. Lübken, Ed. Springer, Dordrecht, Netherlands, 383–408, https://doi.org/10.1007/978-94-007-4348-9_21.

Ern, M., and Coauthors, 2016: Satellite observations of middle atmosphere gravity wave absolute momentum flux and of its vertical gradient during recent stratospheric warmings. *Atmospheric Chemistry and Physics*, **16**(15), 9983–10 019, https://doi.org/10.5194/acp-16-9983-2016.

Faber, A., P. Llamedo, T. Schmidt, A. de la Torre, and J. Wickert, 2013: On the determination of gravity wave momentum flux from GPS radio occultation data. *Atmospheric Measurement Techniques*, **6**(11), 3169–3180, https://doi.org/10.5194/amt-6-3169-2013.

Fetzer, E. J., and J. C. Gille, 1994: Gravity wave variance in LIMS temperatures. Part I: Variability and comparison with background winds. *J. Atmos. Sci*., **51**(17), 2461–2483, https://doi.org/10.1175/1520-0469(1994)051<2461:GWVILT>2.0.CO;2.

Fritts, D. C., and M. J. Alexander, 2003: Gravity wave dynamics and effects in the middle atmosphere. *Rev. Geophys*., **41**(1), 1003, https://doi.org/10.1029/2001RG000106.

Gong, J., D. L. Wu, and S. D. Eckermann, 2012: Gravity wave variances and propagation derived from AIRS radiances. *Atmospheric Chemistry and Physics*, **12**, 1701–1720, https://doi.org/10.5194/acp-12-1701-2012.

Hindley, N. P., C. J. Wright, N. D. Smith, and N. J. Mitchell, 2015: The southern stratospheric gravity wave hot spot: Individual waves and their momentum fluxes measured by COSMIC GPS-RO. *Atmospheric Chemistry and Physics*, **15**(14), 7797–7818, https://doi.org/10.5194/acp-15-7797-2015.

Hoffmann, L., X. Xue, and M. J. Alexander, 2013: A global view of stratospheric gravity wave hotspots located with Atmospheric Infrared Sounder observations. *J. Geophys. Res*., **118**(2), 416–434, https://doi.org/10.1029/2012JD018658.

Holton, J. R., 1983: The influence of gravity wave breaking on the general circulation of the middle atmosphere. *J. Atmos. Sci*., **40**(10), 2497–2507, https://doi.org/10.1175/1520-0469(1983)040<2497:TIOGWB>2.0.CO;2.

Jia, Y., S. D. Zhang, F. Yi, C. M. Huang, K. M. Huang, Q. Gan, and Y. Gong, 2015: Observations of gravity wave activity during stratospheric sudden warmings in the Northern Hemisphere. *Science China Technological Sciences*, **58**(6), 951–960, https://doi.org/10.1007/s11431-015-5806-3.

John, S. R., and K. K. Kumar, 2012: TIMED/SABER observations of global gravity wave climatology and their interannual variability from stratosphere to mesosphere lower thermosphere. *Climate Dyn*., **39**(6), 1489–1505, https://doi.org/10.1007/s00382-012-1329-9.

Khan, A., and S. G. Jin, 2016: Effect of gravity waves on the tropopause temperature, height and water vapor in Tibet from COSMIC GPS radio occultation observations. *Journal of Atmospheric and Solar-Terrestrial Physics*, **138–139**, 23–31, https://doi.org/10.1016/j.jastp.2015.12.001.

Kursinski, E. R., G. A. Hajj, J. T. Schofield, R. P. Linfield, and K. R. Hardy, 1997: Observing Earth's atmosphere with radio occultation measurements using the Global Positioning System. *J. Geophys. Res*., **102**(D19), 23 429–23 465, https://doi.org/10.1029/97JD01569.

Labitzke, K., and B. Naujokat, 2000: The lower Arctic stratosphere in winter since 1952. SPARC Newsletter No. 15, 11–14.

Li, T., T. Leblanc, I. S. McDermid, D. L. Wu, X. K. Dou, and S. Wang, 2010: Seasonal and interannual variability of gravity wave activity revealed by long-term lidar observations over Mauna Loa Observatory, Hawaii. *J. Geophys. Res*., **115**(D13), D13103, https://doi.org/10.1029/2009JD013586.

McHall, Y. L., 1992: Wintertime stratospheric anomalies—Part II: sudden warmings. *Adv. Atmos. Sci.*, **9**(3), 311–322, https://doi.org/10.1007/BF02656941.

Miyahara, S., Y. Hayashi, and J. D. Mahlman, 1986: Interactions between gravity waves and planetary-scale flow simulated by the GFDL "SKYHI" general circulation model. *J. Atmos. Sci*., **43**(17), 1844–1861, https://doi.org/10.1175/1520-0469(1986)043<1844:IBGWAP>2.0.CO;2.

Nappo, C. J., 2002: *An Introduction to Atmospheric Gravity Waves*. 2nd ed, Academic Press, 276 pp.

Nastrom, G. D., A. R. Hansen, T. Tsuda, M. Nishida, and R. Ware, 2000: A comparison of gravity wave energy observed by VHF radar and GPS/MET over central North America. *J. Geophys. Res*., **105**(D4), 4685–4687, https://doi.org/10.1029/1999JD901164.

Ratnam, M. V., G. Tetzlaff, and C. Jacobi, 2004a: Global and seasonal variations of stratospheric gravity wave activity deduced from the CHAMP/GPS satellite. *J. Atmos. Sci*., **61**(13), 1610–1620, https://doi.org/10.1175/1520-0469(2004)061<1610:GASVOS>2.0.CO;2.

Ratnam, M. V., T. Tsuda, C. Jacobi, and Y. Aoyama, 2004b: Enhancement of gravity wave activity observed during a major Southern Hemisphere stratospheric warming by CHAMP/GPS measurements. *Geophys. Res. Lett*., **31**(16), L16101, https://doi.org/10.1029/2004GL019789.

Rocken, C., and Coauthors, 1997: Analysis and validation of GPS/MET data in the neutral atmosphere. *J. Geophys. Res*., **102**(D25), 29 849–29 866.

Sato, K., S. Tateno, S. Watanabe, and Y. Kawatani, 2012: Gravity wave characteristics in the Southern Hemisphere revealed by a high-resolution middle-atmosphere general circulation model. *J. Atmos. Sci*., **69**(4), 1378–1396, https://doi.org/10.1175/JAS-D-11-0101.1.

Schmidt, T., A. de la Torre, and J. Wickert, 2008: Global gravity wave activity in the tropopause region from CHAMP radio occultation data. *Geophys. Res. Lett*., **35**(16), L16807, https://doi.org/10.1029/2008GL034986.

Teng, W. H., C. Y. Huang, S. P. Ho, Y. H. Kuo, and X. J. Zhou, 2013: Characteristics of global precipitable water in ENSO events revealed by COSMIC measurements. *J. Geophys. Res*., **118**(15), 8411–8425, https://doi.org/10.1002/jgrd.50371.

Tsuda, T., T. Inoue, S. Kato, S. Fukao, D. C. Fritts, and T. E. VanZandt, 1989: MST radar observations of a saturated gravity wave spectrum. *J. Atmos. Sci*., **46**(15), 2440–2447, https://doi.org/10.1175/1520-0469(1989)046<2440:MROOAS>2.0.CO;2.

Tsuda T., M. Nishida, C. Rocken, and R. H. Ware, 2000: A global morphology of gravity wave activity in the stratosphere revealed by the GPS occultation data (GPS/MET). *Journalof. Geophysical. Res. earchAtmospheres*, **105**(D6), 7257–7273,

https://doi.org/10.1029/1999JD901005.

Tsuda, T., X. Lin, H. Hayashi, and Noersomadi, 2011: Analysis of vertical wave number spectrum of atmospheric gravity waves in the stratosphere using COSMIC GPS radio occultation data. *Atmospheric Measurement Techniques*, **4**(8), 1627–1636, https://doi.org/10.5194/amt-4-1627-2011.

Uccellini, L. W., and S. E. Koch, 1987: The synoptic setting and possible energy sources for mesoscale wave disturbances. *Mon. Wea. Rev.*, **115**(3), 721–729, https://doi.org/10.1175/1520-0493(1987)115<0721:TSSAPE>2.0.CO;2.

Wang, L., and M. A. Geller, 2003: Morphology of gravity-wave energy as observed from 4 years (1998–2001) of high vertical resolution U.S. radiosonde data. *J. Geophys. Res.*, **108**(D16), 4489, https://doi.org/10.1029/2002JD002786.

Wang, L., and M. J. Alexander, 2009: Gravity wave activity during stratospheric sudden warmings in the 2007–2008 Northern Hemisphere winter. *J. Geophys. Res.*, **114**(D18), D18108, https://doi.org/10.1029/2009JD011867.

Wang, L., and M. J. Alexander, 2010: Global estimates of gravity wave parameters from GPS radio occultation temperature data. *J. Geophys. Res.*, **115**(D21), D21122, https://doi.org/10.1029/2010JD013860.

Wu, D. L., and J. W. Waters, 1996: Satellite observations of atmospheric variances: A possible indication of gravity waves. *Geophys. Res. Lett.*, **23**(24), 3631–3634, https://doi.org/10.1029/96GL02907.

Wu, D. L., and J. W. Waters, 1997: Observations of gravity waves with the UARS Microwave Limb Sounder. *Gravity Wave Processes: Their Parameterization in Global Climate Models*, K. Hamilton, Ed. Springer, 103–120, https://doi.org/10.1007/978-3-642-60654-0_8.

Xu, X. H., J. Luo, and C. Shi, 2009: Comparison of COSMIC radio occultation refractivity profiles with radiosonde measurements. *Adv. Atmos. Sci.*, **26**(6), 1137–1145, https://doi.org/10.1007/s00376-009-8066-y.

Xu, X. H., P. Gao, and X. H. Zhang, 2014: Global multiple tropopause features derived from COSMIC radio occultation data during 2007 to 2012. *J. Geophys. Res.*, **119**(14), 8515–8534, https://doi.org/10.1002/2014JD021620.

Xu, X. H., J. C. Guo, and J. Luo, 2016: Analysis of the active characteristics of stratosphere gravity waves over the Qinghai-Tibetan plateau using COSMIC radio occultation data. *Chinese Journal of Geophysics*, **59**(4), 1199–1210. (in Chinese with English abstract)

Yan, X. P., N. Arnold, and J. Remedios, 2010: Global observations of gravity waves from high resolution dynamics limb sounder temperature measurements: A yearlong record of temperature amplitude and vertical wavelength. *J. Geophys. Res.*, **115**(D10), D10113, https://doi.org/10.1029/2008JD011511.

Zhang, K., E. Fu, D. Silcock, Y. Wang, and Y. Kuleshov, 2011: An investigation of atmospheric temperature profiles in the Australian region using collocated GPS radio occultation and radiosonde data. *Atmospheric Measurement Techniques*, **4**(10), 2087–2092, https://doi.org/10.5194/amt-4-2087-2011.

Zhang, S. D., F. Yi, C. M. Huang, and Q. Zhou, 2010: Latitudinal and seasonal variations of lower atmospheric inertial gravity wave energy revealed by US radiosonde data. *Annales Geophysicae*, **28**(5), 1065–1074, https://doi.org/10.5194/angeo-28-1065-2010.

Zhang, S. D., F. Yi, C. M. Huang, K. M. Huang, Q. Gan, Y. H. Zhang, and Y. Gong, 2013: Latitudinal and altitudinal variability of lower atmospheric inertial gravity waves revealed by U.S. radiosonde data. *J. Geophys. Res.*, **118**(14), 7750–7764, https://doi.org/10.1002/jgrd.50623.